Modelling and numerical simulation of the polymeric extrusion process in textile products

Paola F. Antonietti[a], Nur Aiman Fadel[a], Marco Verani[a]

September 22, 2010

[a] MOX - Laboratory for Modeling and Scientific Computing
Dipartimento di Matematica
Politecnico di Milano
Piazza Leonardo da Vinci 32
I-20133 Milano, Italy
paola.antonietti@polimi.it, nuraiman@gmail.com, marco.verani@polimi.it

Abstract

We present the mathematical modelling and the numerical simulation of the polymer extrusion process of hollow and non-hollow yarns. In particular, the polymeric material flow has been modelled as non-Newtonian, incompressible, isothermal and steady. We attempt to develop a possible strategy for effective die design in profile extrusion and we numerically asses the validity of the model on both academic and real industrial test cases.

Keywords: Free boundary flow, Die-swell, Hollow yarn.
2000 Mathematics Subject Classification. 76D07, 35Q30.

1 Introduction.

Many problems in mechanical engineering and physics are mathematically modelled by partial differential equations defined on domains which are not known a priori. The boundaries of these domains are called free boundaries and must be determined as part of the solution. This means that the problem, apart from the usual unknown quantities (e.g., velocity, pressure), contains additional geometrical unknowns. A technologically and industrially important category of such free boundary problems is formed by the viscous free boundary flow problems, which occurs, for example, in polymer extrusion.

In polymer extrusion of synthetic yarns, the solid polymer is heated beyond the melting point to be enough malleable. Then, the material is forced by one or more screws through a special die to produce a continuous manufactured item (see Figure 1). With such a manufacturing process, it is possible to obtain, for example, sheets, films, pipes, sections, layers and slabs. The aim of this paper is to model and simulate the extrusion

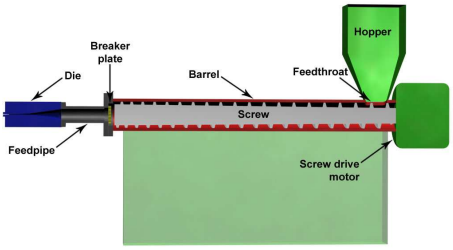

Figure 1: Extrusion process outline.

of hollow and non-hollow yarns. It is known that the cavity affects the fiber insulation property and it improves the fiber permeability, volume and pleating, while reducing the fiber pilling (cf. [3]). We focus on Nylon Polyamide 6 (PA6) yarns because it is the most employed synthetic polymer within the textile industry. The main problem linked to polymer extrusion is the *die-swell* phenomenon which is the increase of polymer section when the polymer leaves the die (see Figure 2). *Die swell* is common among polymeric materials and it is linked to their visco-plastic behaviour (cf. [4]). Because polymers have high molecular weight and high degree of polymerization, they can be considered between an ideal elastic material and an ideal plastic material. Below the principal characteristics of elastic and plastic materials are summarized:

ideal elastic material: under stress it gets deformed, but it recovers to the initial configuration when the stress ends;

ideal plastic material: under stress it gets deformed, and it cannot recover the initial configuration when the stress ends.

Polymers do not behave like these two ideal cases and their behaviour is called *visco-elastic*. At the microscopic level the visco-elasticity is linked to macromolecule properties of the polymer itself. At the macroscopic level a melted polymer reacts as an elastic solid, after being forced through a capillary, and it starts to expand when it leaves the capillary. In a circular pipe, it is formally possible to quantify the entity of the *die swell* using the ratio between the diameter of polymer flux leaving the pipe and the pipe diameter (cf. [5, 6]).

The outline of the paper is the following: in Section 2, we introduce the mathematical model describing the extrusion process; in Section 3 we present the results of a number of numerical experiments, which aim at validating the model on both academic and real industrial test cases.

2 Mathematical model

Let $\Omega \subset \mathbf{R}^d$, $d = 2, 3$ be the computational domain. Let us consider $\Omega_1, \Omega_2 \subset \Omega$ such that $\Omega_2 = \Omega \setminus \bar{\Omega}_1$. The region Ω_1 includes the extrusion die, while Ω_2 includes the free surface (see Figure 3). The Polyamide 6 (PA6) flow has been modelled as non-Newtonian,

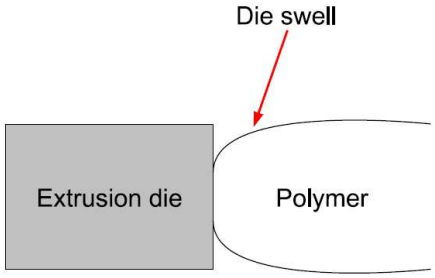

Figure 2: *Die swell* phenomenon.

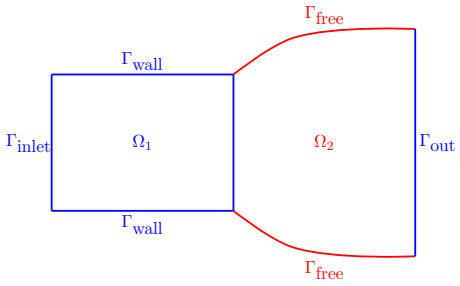

Figure 3: 2D sketch of the boundary conditions.

incompressible, staedy and isothermal. The stationary extrusion process is described by the following free boundary problem (cf. [2, 1, 7, 8]): find the free surface Γ_{free}, the velocity u and the pressure p such that

$$\nabla \cdot \tau - \nabla p = 0 \quad \text{in } \Omega, \tag{2.1}$$
$$\tau = 2\eta(\dot{\gamma})\epsilon(u) \quad \text{in } \Omega, \tag{2.2}$$
$$\nabla \cdot u = 0 \quad \text{in } \Omega, \tag{2.3}$$
$$u = g \quad \text{on } \Gamma_{\text{inlet}} \cup \Gamma_{\text{wall}}, \tag{2.4}$$
$$u \cdot n = 0 \quad \text{on } \Gamma_{\text{free}}, \tag{2.5}$$
$$(-pI + \tau) \cdot n = 0 \quad \text{on } \Gamma_{\text{out}} \cup \Gamma_{\text{free}}, \tag{2.6}$$

where n is the outer normal vector, τ is the stress tensor, $\epsilon(u) = (\nabla u + \nabla u^T)/2$ is the strain tensor, $\dot{\gamma} = \sqrt{2\epsilon(u) : \epsilon(u)}$ is the shear rate, η is the viscosity and g is defined as follows

$$g = \begin{cases} u_{\text{inlet}} & \text{on } \Gamma_{\text{inlet}} \\ 0 & \text{on } \Gamma_{\text{wall}}. \end{cases} \tag{2.7}$$

As a consequence of the non-Newtonian nature of the Polyamide 6, the viscosity $\eta(\cdot)$ depends on the shear rate $\dot{\gamma}$. The most common models in literature are the following:

$$\eta(\dot{\gamma}) = \text{costant} \quad (Newtonian\ model); \tag{2.8}$$

$$\eta(\dot{\gamma}) = \eta_\infty + \frac{\eta_0 - \eta_\infty}{(1+\lambda^2\dot{\gamma}^2)^{(1-n)/2}} \quad (Bird - Carreau\ model); \tag{2.9}$$

$$\eta(\dot{\gamma}) = \eta_\infty + \frac{\eta_0 - \eta_\infty}{1+(\lambda\dot{\gamma})^n} \quad (Cross\ model), \tag{2.10}$$

where λ is the characteristic time, n the pseudo-plastic index, η_0 and η_∞ are the viscosities of the two Newtonian plateau. The momentum equation is then highly coupled with the viscosity constitutive equation. In the rest of this work we will make use of the Cross model (2.10) (see Table 2 for the numerical values of the parameters).

3 Numerical experiments

The numerical experiments have been performed by using commercial softwares. The mesh has been generated by using the software Gambit [11]. To handle the finite element approximation to the free surface problem (2.1)-(2.6), we have employed the CFD solver POLYFLOW [12] which is well suited to handle problems involving complex non-Newtonian rheologies, and where advanced numerical techniques to deal with free surfaces are available to accurately simulate the extrusion process. Because the border of the extrudate changes its shape during the simulation, in addition to the solution of the (unknown) position of the free surface, the nodes of the mesh need to be relocated. We have employed OptiMesh [10], an anisotropic automatic mesh adaptation module available in POLYFLOW, which is well suited to take into account the very large deformations encountered in the extrusion process besides drastically reducing mesh generation efforts.

The numerical experiments are divided into two categories: academic and industrial test cases.

3.1 Academic Test Case

We test the mathematical model introduced in Section 2 on an academic test case. The 3D geometry considered in this set of experiments is reported in Figure 4 (left), while the data employed are reported in Table 1. Proper setting of the quality of the

Table 1: Academic test case: rheological parameters.

Parameter	Value
η_0	1 Pascal
η_∞	0 Pascal
λ	0.2 s
n	0.3
volumetric flow rate at the inlet	$1.0 * 10^{-5}\text{m}^3/\text{s}$

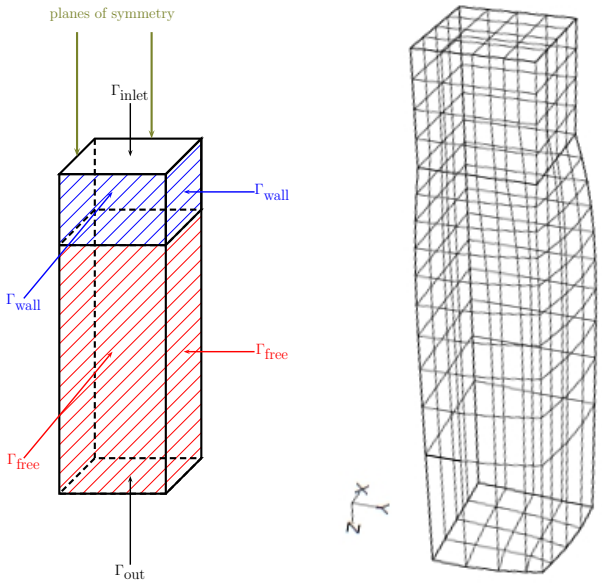

Figure 4: Academic test case. Geometry (left) and sample of the mesh (right).

finite element mesh is of crucial importance to get successful extrusion simulation, since insufficient mesh density can indeed deteriorate the quality of the results. The mesh is built using wedge or hexahedral elements and, in order to properly handle the free surface modelling with the moving mesh algorithm in the deformation surface zone (i.e., where the polymer leaves the die), it is mandatory to have a sufficiently refined grid near the die exit. In particular, an improper mesh density where the most intensive deformation takes place might cause a non-convergence of the algorithm. A sample of the mesh used in the 3D simulation is shown in Figure 4 (right), where the mesh size of the elements increases along the z-axis (i.e., far from the die exit).

The computed pressure is reported in Figure 5 (left). Notice that, the die swell occurs (as expected) just after the polymer leaves the die. The computed velocity vectors are show in Figure 5 (right). Notice that, after the die exit, a rearrangement of the velocity field takes place, and according to the kinematic condition $u \cdot n = 0$, the velocity field is tangential to the free surface.

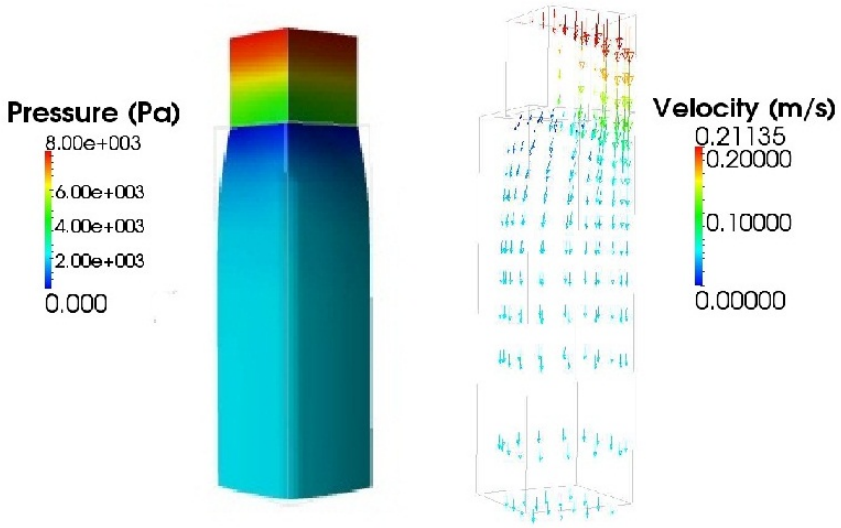

Figure 5: Academic test case. Computed pressure (left) and velocity (right).

3.2 First Industrial Case: Non-hollow Yarn

We consider the simulation of the extrusion of a standard industrial non-hollow yarn. The geometry of the single hole in the extrusion die is reported in Figure 6. In this second set

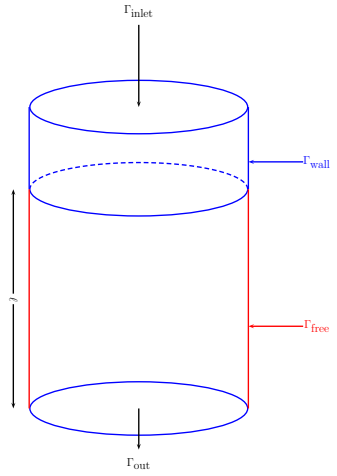

Figure 6: Non-hollow yarn. Geometry of the single hole in the extrusion die.

of experiments we have considered the PA6 rheological parameters [9] and we take the mass flow rate at the inlet equal to $2.2 * 10^{-3}$Kg/s. The data for this set of experiments are summarized in Table 2. We have considered several values of the height ℓ of the free surface region (see Figure 6): $\ell = 3.0 * 10^{-2}, 1.0 * 10^{-2}, 5.0 * 10^{-3}, 1.0 * 10^{-3}$ m. In all the cases, we observed that the *die-swell* happen immediately after the polymer reaches

Table 2: Non-hollow yarn: PA6 rheological parameters.

Parameter	Value
η_0	162.18 Pascal
η_∞	0 Pascal
λ	0.0003244 s
n	0.9493
Mass flow rate at the inlet	$2.2 * 10^{-3}$Kg/s

the air. Then, it is possible to consider reasonably little values of ℓ without altering the quality of the numerical results. In Figure 7 we show the computed extrudate section and profile for $\ell = 5.0 * 10^{-3}$ m; whereas the extruded profiles obtained with $\ell = 1.0 * 10^{-3}$ m and $\ell = 3.0 * 10^{-2}$ m are shown in Figure 8. The legends refer to the distance (in meters) from the symmetry center. In Table 3, for different values of ℓ, we report the computed

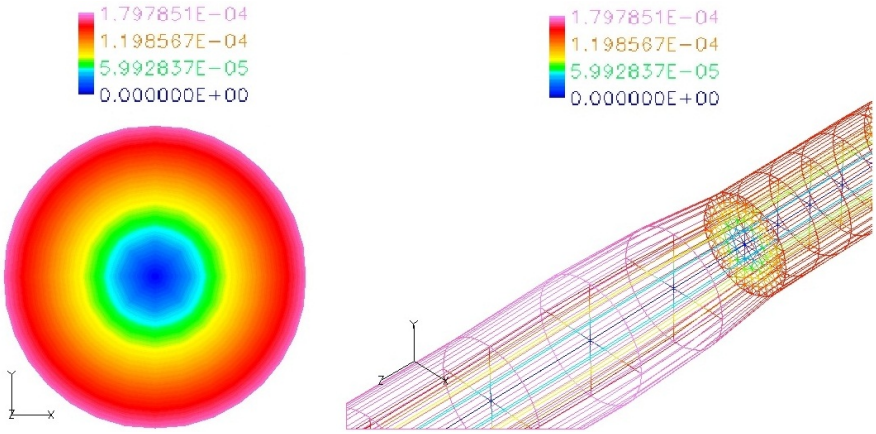

Figure 7: Non-hollow yarn. Extrudate section and profile, $\ell = 5.0 * 10^{-3}$ m. The legends refer to the distance (in meters) from the symmetry center.

radius r_{ext} of the extrudated polymer at the outlet. We also report the quantity r_{ext}/r_{die}, being $r_{die} = 1.45 * 10^{-5}$ m the radius of the die, which represents the amount of *die-swell* in percentage. It can be seen that the radius of the extrudate polymer is greater than that of the die, and, taking the average of the computed data, the die-swell ratio is approximately 21%. In order to validate our numerical computations, we have compared the numerical results with the experimental data (reported in the last row of Table 3). For the acquisition of the experimental data, since we want to measure the amount of die-swell as the polymer reaches the air and before it turns to the solid state, we have proceeded as follows. The picture shown in Figure 9, reporting a detail of the industrial extrusion of non-hollow yarn, has been taken so that the image resolution is $1.3 * 10^{-5}$ m per pixel, with a tolerance of approximately one pixel. Next, by using an image processing software, the experimental extruded radius has been estimated to be $1.82 * 10^{-4}$ m $\pm 1.3 * 10^{-5}$ m. All the numerical results are in agreement with the experimental data up to a percentage

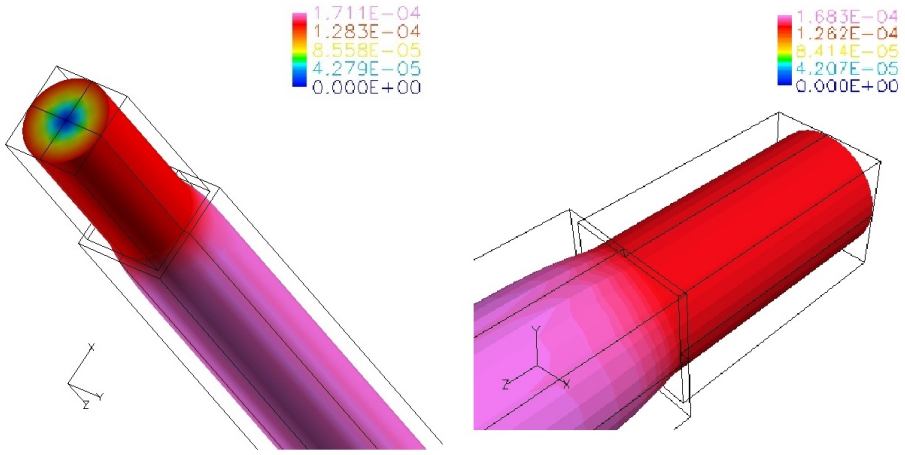

Figure 8: Non-hollow yarn. Extruded profiles $\ell = 3 * 10^{-2}$ m (left) and $\ell = 1 * 10^{-3}$ m (right). The legend refers to the distance (in meters) from the symmetry center.

Table 3: Non-hollow yarn: Extruded radius r_{ext} and extrudate swell ratio r_{ext}/r_{die} for different values of ℓ.

	r_{ext}	r_{ext}/r_{die}
$\ell = 1.0 * 10^{-3}$ m	$1.68 * 10^{-4}$ m	1.16
$\ell = 5.0 * 10^{-3}$ m	$1.80 * 10^{-4}$ m	1.24
$\ell = 1.0 * 10^{-2}$ m	$1.84 * 10^{-4}$ m	1.27
$\ell = 3.0 * 10^{-2}$ m	$1.71 * 10^{-4}$ m	1.18
Experimental data	$1.82 * 10^{-4}$ m $\pm$ $1.3 * 10^{-5}$ m	1.26$\pm$0.09

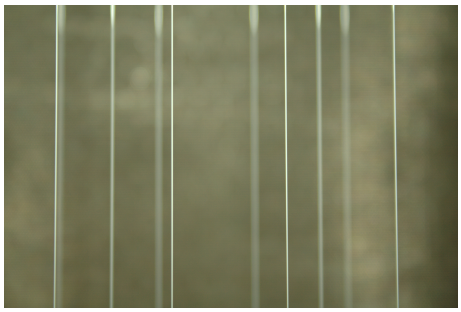

Figure 9: Non-hollow yarn. Zoom of industrial extrusion of PA6 yarn. (Courtesy of RadiciYarn S.p.A.).

tolerance of 10%, and confirm the accuracy of our model. More precisely, the results obtained with $\ell = 5.0 * 10^{-3}$ m and $\ell = 1.0 * 10^{-2}$ m match very well the experimental data, whereas the results obtained with $\ell = 1.0 * 10^{-3}$ m and $\ell = 3.0 * 10^{-2}$ m slightly underestimates the extrudate swell ratio. The latter behavior could be explained as follows: the choice $\ell = 1.0 * 10^{-3}$ m is too restrictive since the *die-swell* phenomenon is probably still active; whereas for $\ell = 3.0 * 10^{-2}$ m, the computational mesh has to be chosen coarse enough to face the computational costs, and this probably affects the quality of the numerical results.

3.3 Second Industrial Case: Hollow Yarn

The second industrial test case concerns the numerical simulation of the extrusion process driven by the trilobe die depicted in Figure 10 (left). The computed extruded polymer

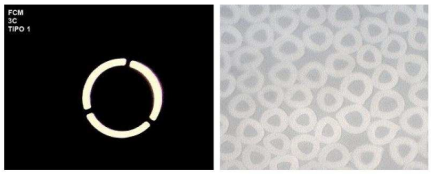

Figure 10: Trilobe die. Die Geometry (left) and extruded polymer profiles (right). (Courtesy of RadiciYarn S.p.A.).

profile is shown in Figure 11 (right); a comparison between the die profile (colored according to the distance form the symmetry center) and the profile of the extruded polymer (in red) is shown in Figure 11 (left). For completeness, we also report the experimental results (Figure 10 (right)) that show the section of the trilobe yarn obtained by industrial extrusion. Moreover, we address the study of the pressure and velocity distribution in

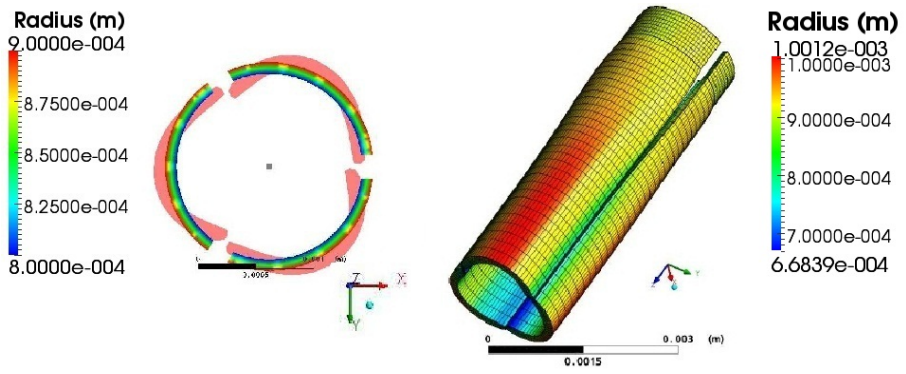

Figure 11: Trilobe die. Computed extruded polymer profiles. The legends refer to the distance (in meters) from the symmetry center.

the die and in the extruded yarn. The computed pressure is reported in Figure 12 (left).

We clearly observe that, as expected, the pressure decreases almost linearly within the die, and it is equal to the external pressure as the polymer reaches the free boundary. We also notice that the numerical pressure obtained at the die entrance is in agreement with the typical values ($10^7 - 10^8$ Pascal) measured during industrial extrusion. Concerning velocity distribution, Figure 12 (right) showns the radial component of velocity which can be used to identify the region where the *die swell* takes place. Indeed, it is well known that the *die-swell* phenomenon is associated with the changes in the velocity profiles of the flowing melt occurring at the die exit. As the results reported in Figure 12 (right) show, the maximum value of radial component of the velocity is located in the die-swell region, where the polymer expansion occurs, while the zero value is attained when moving away from such region. Finally, we also investigated how the internal and external

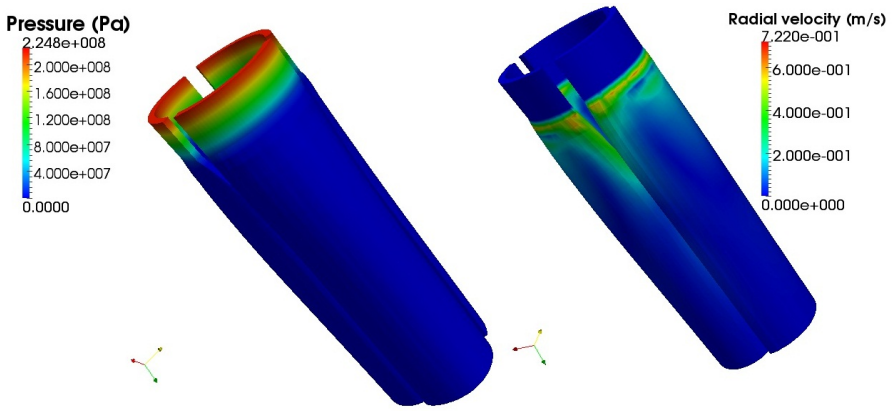

Figure 12: Trilobe die. Computed pressure and radial velocity magnitude.

radii of the yarn vary along the distance from the die. More precisely, we have denoted by $r_{\mathrm{i,m}}$ and $R_{\mathrm{e,m}}$ the internal and external radii of the yarn, respectively, measured (with respect to the symmetry center) at the middle of the lobe; analogously, $r_{\mathrm{i,s}}$ and $R_{\mathrm{e,s}}$ denote the same quantities measured at the right side of the lobe (cf. Figure 13 (left)). Figure 13 (right) shows the computed internal and external radii as a function of the distance from the die. On one hand, we can observe that, while the *die-swell* phenomenon takes place, the internal and external radii $r_{\mathrm{i,m}}$ and $R_{\mathrm{e,m}}$, measured at the midpoint of the lobe, increase monotonically, and then they remain constant. On the other hand, the internal and external radii $r_{\mathrm{i,s}}$ and $R_{\mathrm{e,s}}$, measured at the right side of the lobe, have a more complex behaviour: they initially increase, then decrease up to a plateau value, and the lobe turns into the (non-regular) shape depicted in Figure 11 (left). Such a behaviour could be explained in terms of the rearrangement of the velocities which take place on both the internal and the external profile, as well as on the straight face. This numerical results, together with the extruded polymer profile reported in Figure 11, confirm the experimental data (cf. Figure 10) and show how the trilobate die geometry does not allow to obtain hollow yarns with outer circular profiles, but rather a "triangular" shape. Thus, the "naive" trilobate geometry is not suitable for industrial hollow yarn production on

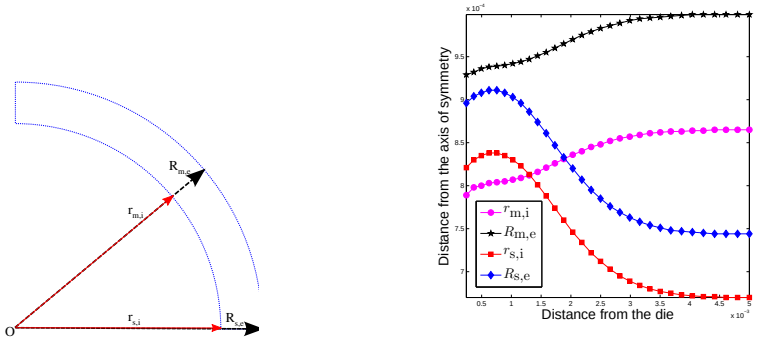

Figure 13: Trilobe die. Left: internal and external radii of the yarn. Right: computed internal and external radii of the yarn versus the distance from the die.

large scale, since a regular circular shape with the fewest possible variations is mandatory in real industrial applications.

As a consequence, from the industrial point of view, it becomes crucial to possess a numerical tool enabling to design "optimal" dies, which guarantee hollow yarns with prescribed circular sections. This topic is named *inverse die design* and refers to the issue of automatically adjust the die lip to extrude a certain goal profile despite the deformations encountered inside the free jet. The efficient solution of such an inverse problem is crucial for industrial applications as it reduces trial-and-error testing, thus resulting in a considerable saving of time and economic resources. We addressed the (inverse) problem of predicting the optimum die profile-shape and dimensions, to obtain a circular hollow yarn. To achieve this goal, we used the method of Inverse Extrusion available in the CFD code POLYFLOW [12], which is capable to optimize the die design and ultimately to achieve the desired profile and dimensions of the extrudate. Firstly, we investigated a bilobe geometry (the topology of the die is a priori fixed). However, in order to consistently manufacture a high-quality product, the bilobe die seems not to be the most effective choice. Indeed, due to the small size of the die (notice that the characteristic length is of order 10^{-4} meters) and to the high pressure reached by the polymer before the die exit, it might not have enough tensile strength since it is made only by two (micro) pieces. We therefore tested a different topology, i.e., a quadrilobe geometry, which seems to be more suited for industrial applications. This topic will be extensively addressed in a future work.

4 Conclusion

We undertook the mathematical modelling and the numerical simulation of the polymeric extrusion of hollow and non-hollow yarns. The polymeric material flow has been modelled as non-Newtonian, incompressible, isothermal and steady, and the Cross rheological law has been employed as constitutive model for the viscosity. The accuracy of

the adopted method to approximate the solution to the polymeric extrusion problem has been numerically addressed.

5 Acknoledgements

We are grateful to Alessandro Veneziani, who introduced us to the topic of mathematical and numerical modelling of textiles. P.A., and M.V. have been funded by the project RBIP06HF8S "*Materiali e Tecnologie innnovativi per il Tessile Italiano*", and by the project HOT-FDI "*Hollow and Transparent Fibers Design for Industries*". N.F. has been supported by the project "*Metodi Numerici per la Simulazione di Processi di Estrusione*" funded by the "Fausto Saleri" SIMAI prize.

References

[1] J. W. Barrett, E. Süli, Existence of global weak solutions to some regularized kinetic models of dilute polymers, *Multiscale Model. Simul.* 6 (2007), 506–546

[2] J. W. Barrett, C. Schwab, E. Süli, Existence of global weak solutions for some polymeric flow models, *Math. Models Methods Appl. Sci.* 15 (2005), 939–983.

[3] W.-S. Lee and H.-Y. Ho, Experimental study on extrudate swell and die geometry of profile extrusion, *Polymer engineering and science*, vol. 40, no. 5, pp. 1085–1094, 2000.

[4] R. Tanner, A theory of die-swell, *Journal of polymer science: part A-2*, vol. 8, pp. 2067–2078, 1970.

[5] D. L. Han-Xiong Huang and Yan-Sheng Miao, Numerical prediction and experimental validation of viscoelastic annular swell, *Advances in Polymer Technology*, vol. 25, no. 4, pp. 259–269, 2006.

[6] T. K. Yasuhiko otsuki and K. Funatsu, Numerical simulations of annular extrudate swell of polymer melts, *Polymer engineering and science*, vol. 37, no. 7, pp. 1171–1181, 1997.

[7] E. Mitsoulis, Three-dimensional non-newtonian computations of extrudate swell with the finite element method, *Comput. Methods Appl. Mech. Engrg.*, vol. 180, pp. 333–344, 1999.

[8] E. Mitsoulis, Annular extrudate swell of pseudoplastic and viscoplastic fluids, *Journal Non-Newtonian Fluid Mech.*, vol. 141, pp. 138–147, 2007.

[9] A. Guštin and A. Zupančič, Pressure drop estimation for Polyamide 6 flow through spinnerets and filters, *Journal of Applied Polymer Science*, vol. 100, pp. 1577–1587, 2006.

[10] W.G. Habashi, J. Dompierre, Y. Bourgault, M. Fortin and M.-G. Vallet, Certifiable Computational Fluid Dynamics Through Mesh Optimization, Invited Paper in Special Issue on Credible Computational Fluid Dynamics Simulation, *AIAA Journal*, Vol. 36, No. 5, pp. 703-711, 1998.

[11] *http://www.gambit.it*

[12] *http://www.fluent.com/software/polyflow/extru.htm*